Fabrication of High Band Gap Kesterite Solar Cell Absorber Materials for Tandem Applications.

Authors

Thierry Kohl[1,2,*], G. Brammertz[1,2], J. de Wild[1,2], M. Neuwirth[4], M. Meuris[1,2], J. Poortmans[1,3,5], B. Vermang[1,2]

[1] Institute for Material Research (IMO), Hasselt University (partner in Solliance & EnergyVille), Agoralaan gebouw H, Diepenbeek, 3590, Belgium
[2] Imec division IMOMEC (partner in Solliance & EnergyVille), Wetenschapspark 1, 3590 Diepenbeek, Belgium.
[3] Imec (partner in Solliance & EnergyVille), Kapeldreef 75, Leuven, 3001, Belgium
[4] Institute of Applied Physics, Karlsruhe Institute of Technology, Wolfgang-Gaede Straße 1, 76131 Karlsruhe, Germany.
[5] Department of Electrical Engineering, KU Leuven, Kasteelpark Arenberg 10, 3001 Heverlee, Belgium

Highlights

- We created CZGSSe absorber layers with sulfur inclusion going from 30% to 100%.
- These absorbers have a respective band gap of 1.45 eV to 2.0 eV.
- The results from these annealing procedures were very well reproducible.
- The sulfur inclusion is very slow. The first 30min both CZGSe and CZGSSe coexist.
- It is impossible to have a uniform absorber layer with less than 30% S inclusion.

Abstract

Using the thermal annealing of evaporated metallic precursors in successive H_2Se and H_2S atmospheres, it was possible to reproducibly manufacture kesterite absorber material for solar cell applications with a sulfur content varying from 30% to 100%. Respective band gaps for these sulfur inclusions were measured at approximately 1.45eV and 2.0eV. A recipe was devised for which results could be reproduced within an error margin of ±5% and the influence of the H_2S pressure during the post sulfurization was negligible on all measurable and observable parameters. The evolution of the S/Se ratio in the sample was observed to be linearly dependent on the annealing time. It was also observed that at very early stages of the post-sulfurization, both the original $Cu_2(Zn,Ge)Se_4$ (CZGSe) and a primary $Cu_2(Zn,Ge)(S,Se)_4$ (CZGSSe) phase with a sulfur inclusion of ~30% coexist in the sample. The (112) x-ray diffraction (XRD) reflection of the CZGSe phase progressively disappears in favor for the first mixed CZGSSe phase. Using grazing incidence-XRD, the S/Se ratio was shown to be inhomogeneous. Indeed, the XRD measurement of the top layers led to the calculation of higher sulfur inclusions than was the case when measuring the bulk material. Top-scanning electron microscopy (SEM) as well as cross-SEM measurements were taken in order to determine the impact of the sulfur inclusion on the crystal growth and the overall quality of the produced absorber layers. The obtained images revealed a reduction in crystal size and the appearance of numerous holes in the layer as the S/Se ratio is increased.

Keywords

Kesterite, Absorber Material, Precursor annealing, High band gap, Thin film solar cell, Tandem, CZGS.

Introduction

The total amount of energy generated by solar energy has been very rapidly increasing these past few years. The global capacity has been multiplied by 4 in the last five years [1] and is expected to keep increasing in the coming years with the emergence of renewable energy favorable policies in many countries on the planet. It will be necessary, in the years to come, to be able to consistently produce large amounts of highly efficient solar cells to keep up with the demand. Traditional Si-based photovoltaic (PV) setups might still occupy an important place on the global market but could very well be replaced by Thin Film (TF) PV technologies with the emergence of building-integrated (BI) PV solutions. Indeed, TFPV can be implemented on a wide variety of solid or flexible substrates, which makes them interesting for BIPV applications. Classical TFPV materials like $Cu(In,Ga)(S,Se)_2$ (CIGS) and CdTe, on the other hand, could be limited in the long run, due to scarcity of elements like In and Ga or the toxicity of Cd.

Due to this, in recent years, kesterite absorber materials, most prominently represented by $Cu_2ZnSn(S_xSe_{1-x})_4$ (CZTS) [2-6], have been largely studied as a replacement thin film absorber for solar cell applications. The main advantage this type of materials provides is the non-toxic and earth abundant nature of the elements involved in their production. However, no matter how good a certain material might be, the efficiency of the subsequently produced solar cell is intrinsically limited by what is commonly known as the Shockley-Queiser limit, which predicts the theoretical maximal values of the various solar cell parameters [7]. One way to outperform this theoretical limit is to create cells using multiple p-n junctions, commonly known as tandem cells. In order for this type of architecture to work, it is necessary to have a top-cell with a higher band gap than the one of the regular bottom cell. In addition to the commonly used S/Se replacement [8], [9], elemental replacement of Sn by Ge in the CZTS structure has been investigated as a possible solution to increase the band gap of the absorber material [8]. In the case of the selenium phase of the tin kesterite, $Cu_2ZnSnSe_4$, the band gap has been shown to vary from 1.1 eV to 1.4 eV when varying the Ge/(Sn+Ge) ratio from 0 to 1 [8]. Subsequently, $Cu_2ZnGe(S_xSe_{1-x})_4$ (CZGS(e)) [10], with a band gap of 1.4 eV to 2.0 eV [8], [11] is a promising candidate to produce a high band gap kesterite material to be used in the top cell of a tandem thin film solar cell. The ideal band gap for the top cell is situated between 1.6 eV and 1.8 eV [12].

The most predominantly used methods to produce CZGS are wet processes (e.g. [13], [14]) or annealing of metallic precursors using elemental Se and S sources [15-18]. These methods allow for a high throughput. In the present case, it was decided to produce samples through annealing of metallic precursors, but to perform the annealing in gaseous atmosphere (H_2Se and H_2S). This approach was chosen in the hope that it would allow for an optimal control of the concentration of elements in the annealing reactor.

Experimental methodology

The metallic precursors are deposited on a 5cm x 5cm Soda-Lime Glass substrates coated with a 150 nm Si(O,N) diffusion barrier and a 400nm Mo back contact. The deposition is performed by e-beam evaporation in a Pfeiffer E-Gun PLS 580. A stack of a 200nm layer of Ge, a 125nm layer of Zn, a 170nm thick layer of Cu is deposited by evaporation from solid, 99.999% pure, metal pellet crucibles in vacuum.

Before the samples are processed any further, they are split into two 2.5cm x 5cm samples. Annealing was done in an Annealsys AS-one annealing oven, which was first cleaned at 50 degrees by being cyclically purged and pumped down. As selenium source, H_2Se gas was used, which allowed for a better control of the pressure in the chamber by adjusting the flow rate in and out of the chamber. During the ramping up to the selenization temperature of 460°C at a 1°C/s rate a continuous flow of 140sccm of H_2Se is filled into the reaction chamber. At

the end of this step, the gases are pumped out of the chamber again. The selenization itself is a continuous flow of 200sccm of H_2Se at 460°C until the chamber reaches a pressure of 99 kPa. After selenization, the chamber is emptied of all residual gases again before the system is ramped up to 510°C, for the sulfurization step. Sulfurization was done with H_2S gas. The pressures, flow rates and annealing times were varied to control the S concentration in the final layer. During this sulfurization step, the chamber is cyclically emptied and refilled with fresh H_2S gas. Once the desired sulfurization time is over, the reactor is drained, purged and the samples are cooled down to 150°C under a continuous flow of 2000sccm of N_2 and H_2 before being extracted from the oven.

Photoluminescence (PL) response of the absorber layer was measured in a near-infrared compact fluorescence lifetime spectrometer from Hamamatsu. Two room temperature measurements were taken at respective laser powers of 1mW and 45 mW.
The band gap was measured by reflection spectral response, in which the material is submitted to a light beam with a wavelength varying from 300 nm to 1200 nm. The band gap could then be determined by using the method developed by Tauc et al. [19] or by linear fitting of the reflection edge, the latter being used predominantly in the present work.

The composition of the absorber material was investigated by using a PANalytical X'Pert x-ray diffractometer with a Cu-Kα x-ray source. For the compositional analysis, a very quick (6 min) Bragg-Brentano scan was performed, from $2\theta = 10°$ to 90°. The phase identification was done by comparison with reference diffractograms. The S/Se ratio was numerically calculated using the relative shift of the (112) CZGSSe peak maximum and its position relative to the CZGSe and CZGS reference positions. To do so, a linear shift as a function of the S inclusion was assumed. Additional GI-XRD scans were performed to get information about the in-depth composition of the sample. The incidence angle was varied from 0.1° to 1.0°.

Top-SEM measurements were performed on a Philips XL-30 SEM to investigate the quality of the film as well as verify its horizontal homogeneity by using energy dispersive spectroscopy (EDS). EDS measurements were taken on 3 separate 25 μm² areas on the sample and the average and standard deviation of the results from these measurements were calculated. Cross-SEM measurements were performed using the in-lens detector on a Carl Zeiss Supra 55VP, using a 2 kV acceleration voltage at the Karlsruhe Institute of Technology.

Results and discussion

Before developing the recipe used to obtain the samples presented in this work and the results that are linked to them, an annealing recipe with one single filling of the reaction chamber with H_2S gas was used. It appeared that reducing the sulfur inclusion after a 120 min annealing period was possible by reducing the amount of H_2S pressure injected into the reactor prior to annealing, as shown in fig 1a). In this figure, the sulfur inclusion, as determined from XRD measurements, is plotted as a function of the pressure of H_2S in the reaction chamber. Although it was possible to control the S/Se ratio by adapting the H_2S pressure, the amount of secondary phases in the sample was high and the creation of the CZGS phase was not optimal. This observation can be explained by equilibrium reaction mechanics as it was done for the tin kesterite (CZTS) [20], [21] given that some of the secondary compounds like GeS are volatile [22]. Indeed, the low H_2S pressures during sulfurization could lead to a deficit of S during the reaction and ultimately force the reaction into the direction of the production of secondary phases, rather than the production of the quaternary kesterite compound. Knowing this, by increasing the available amount of S during sulfurization, it should be possible

to create an excess of products and lead to the creation of an increased amount of the desired kesterite phase. Based on this assumption, the recipe as it was described in the experimental section was developed. The first trials showed immediate results through a highly reduced formation of secondary phases and defects. The improved quality of the layer is best visible on a direct comparison of the PL spectra as presented in fig. 2. After including the purge and refill steps into the annealing recipe, a second series of trials was launched to determine the impact of the H_2S pressure on the overall sulfur inclusion at the end of this new process. As can be seen in figure 1b), no clear trend could be determined and the resulting sulfur inclusion is relatively constant for all the applied pressures. The pressure of 50 kPa is the only exception as the resulting S/Se, which suggests an effect on the sulfur inclusion after 50 min. This could be explained by the fact that a higher amount of H_2S atoms in the reactor chamber could slow down the extraction of the Se atoms during their replacement by S atoms in the kesterite structure, eventually limiting the sulfur inclusion. PL measurements performed on this set of samples also highlighted a very pronounced tailing effect at lower photon energies, subsequently broadening the PL peak and making it less sharp. Since the origin of this band tailing could not be determined conclusively and it is an undesirable effect, it was determined that the optimal range of pressures for the sulfurization of the sample was from 15 kPa to 40 kPa.

Using the process described in the previous section, a link between the sulfurization time and the final amount of sulfur in the absorber layer could be determined. This link is exemplified in fig. 3a). As can be seen, the relation between sulfur inclusion and sulfurization time can be approximated to be linear up to the point at which the sulfur inclusion saturates at values approaching 100%. The sulfur inclusion values being determined by numerical calculations can be subjected to uncertainties, that is why they were double checked using results from EDS measurements. These showed a reasonably good correspondence between the two methods. A selection of EDS results, reprising cation compositions and S/Se ratios of relevant samples, is presented in table 1. A good homogeneity over the whole surface of the sample could be observed on all the measured samples as well.

The results in table 1 show that the S inclusion calculated from the XRD and EDS results match reasonably well. It is also apparent that the Cu/(Zn+Ge) ratio is typically close to 0.9 with very slight variations around this value. However, the Zn/Ge ratio varies slightly more but is in general situated close to 1.15.

A second observation that can be drawn from fig. 3a) is that the results obtained by using this type of annealing process can be very easily reproduced. In most cases, values of sulfur inclusion stay within an error margin of ±5% when repeating a specific recipe multiple times. An example of results of a reproducibility test can be found in table 2.

As can be seen in table 2, a sample annealed for 50 min at 30 kPa H_2S atmosphere with a 6 min preselenization and a 50°C preheating has an average sulfur inclusion of 53.3 % and the standard deviation of the presented set of samples is 3.2%.

It is also visible, in fig. 3a), that the points corresponding to very short sulfurization times, i.e. 10 and 20 min, do not fully fit the linear trend set by the rest of the data. Indeed, it appears that the actual sulfur inclusion is about 10-15% lower than what could be expected if the points followed the linear trend set by the rest of the data. An investigation into the evolution of the composition of the kesterite absorber film for the low annealing lengths showed that, in the very early stages of the sulfurization of the sample,

the layer is still mostly composed of pure CZGSe. Over time, the XRD peak corresponding to this phase slowly disappears in favor of a first mixed CZGSSe phase. It appears that this first mixed phase of the material has a sulfur inclusion of about 30%. These results are presented in fig. 4. It also becomes apparent that in order to achieve the complete transformation of the CZGSe material into this initial mixed CZGSSe phase, it is necessary to anneal the sample in H_2S atmosphere for at least 30-35 min. This could mean that the replacement of Se by S in the CZGS kesterite matrix is a rather slow process. Moreover, it could mean that the sulfur inclusion range from 0% to 30% is not achievable using this type of sulfurization approach.

Fig. 5 gives the full XRD diffractograms of 3 of the graphs presented in fig.4. Namely, the samples with a respective S inclusion of approximately 0%, 50%, and 100% are depicted. It can be seen on this graph that the material produced through our annealing process is mostly phase pure germanium kesterite. However, it appears that a small amount of a Zn secondary phase is also produced. This phase is mostly visible through small shoulders on the (112) reflection of the kesterite. It also seems that at the same time the kesterite sulfurizes, the ZnSe also sulfurizes to ZnS over time, since on the diffractogram of the un-annealed sample, the shoulder on the (112) reflection can be identified as ZnSe, whereas on the fully sulfurized samples, the shoulder corresponds to ZnS.

As it could be expected from previously obtained results in the cases of CIGS and CZTS [23], it was equally observed in the present case that the band gap of the material evolves linearly with the replacement of Se by S in the crystal structure, this can be seen in fig. 3b). Values of the band gap, that were observed in the framework of this work, vary from 1.35 eV to 2.0eV for a pure CZGSe and CZGS material respectively, which is reasonably in line with previous predictions and results [8],[11]. The band gap of pure CZGSe being predicted at 1.4 eV [11], it is, however, probable that the band gap of the samples with the lowest sulfur inclusion (0%-20%) in fig. 3a) were underestimated. Indeed, a band gap value that is almost constant for sulfur inclusions from 0% to 30% would make more sense given the difficulties to achieve sulfur inclusions below 30% observed in figure 4. Given the linear evolution of the band gap with sulfur inclusion, in order to produce a material with a band gap comprised between 1.6 eV and 1.8 eV, it is necessary to achieve sulfur inclusion varying between 50% and 80%. The corresponding sulfurization times in the case of the present process are from 50 min to approximately 70 min.

The peculiar shape of the XRD peaks observed on fig. 4, especially the heavy tailing on the peaks of the higher annealing times, led to further investigation on the exact composition of the sample along its thickness. To that end, GI-XRD was performed on selected samples in order to see how the sulfur content evolves over the thickness of the sample. The diffractograms for increasing incidence angles of a ~50% CZGSSe sample are presented in fig. 6. It is clearly visible that the sulfur content is much higher in the top layers of the absorber than in the bulk. Indeed, when looking at the numbers determined from numerical analysis of the XRD data, it becomes apparent that there is a sulfur gradient of about 20% between the top layer and the bulk. This gradient is problematic since it goes against the proper band alignment, by steadily increasing towards the SCR and the interface with the CdS. This increase in band gap as we go towards the p-n junction is bound to be problematic for charge carrier collection in the finished solar cell. Given the existence of the sulfur gradient in the absorber layer as well as the observation of the progressive disappearance of the CZGSe peak in fig.4, it is likely that both are a consequence of the process itself.

Indeed, since the sulfur source (H_2S) is always in contact with the top layer of the material, sulfur atoms must diffuse through the whole layer in order to sulfurize the lower layers of the

thin film. Consequently, layers that are in contact with sulfur for an extended timespan would showcase higher degrees of sulfur inclusion compared to the ones for which the actual availability in S atoms is limited by the diffusion speed of said atom through the absorber material.

In order to qualitatively determine the effect of the sulfur inclusion on the aspect of the absorber layer, Top-SEM images were taken, which are presented in fig. 7. Accompanying EDX measurements showed compositional results, in particular the S/Se ratio, in good correspondence with the ones that were numerically determined from the XRD data, see tab.1. Other samples, processed in the same annealing runs and/or using the same recipes as the ones used for top-SEM, were used for the production of high resolution cross-SEM pictures. The images, resulting from these measurements, are visible in fig. 8.

In the case of the top-SEM images, it appears that the surface is initially covered with relatively big crystals, with approximate sizes situated between 0.5 μm and 1 μm. These crystals are easily distinguishable and showcase sharp edges and defined forms. As more sulfur is added into the layer - see evolution on fig. 7a)-d) - it appears that the crystals are deteriorated: edges become increasingly less sharp and the general shape of the crystals becomes difficult to discern and less defined. In addition, holes appear on the surface of the absorber layer and become more numerous and increase in size as more sulfur is added into the layer. This observation was confirmed by the results presented in fig. 8, related to the cross-SEM measurements. Indeed, in fig. 8a), the pure Se absorber layer appears as a full and almost continuous layer. Holes are scarce and crystals are big and cover most of the thickness occupied by the absorber layer. As the S/Se ratio increases, holes in the layer become more present and increase in size. It is also visible on the cross-SEM images that crystals are smaller in the topmost layers of the absorber, compared to the lower layers. This observation is in keeping with the previous observation that the sulfur content in the layer is not homogeneous. Layers that are closer to the surface are more heavily exposed to H_2S during the sulfurization and are consequently more heavily sulfurized. This increased sulfur inclusion is then visible on the micrograph through the presence of smaller crystals in the topmost layers of the absorber.

The holes that were observed on both types of images could be problematic, as they could lead to short-circuits in the solar cells and lead to shunting related efficiency losses in the solar cells.

Independently of the sulfur content, the CZGS absorber layer appears to have a very rough surface. This roughness could be problematic when depositing the buffer layer in the final production steps of the creation of the finished solar cells. The rough interface could have a negative impact on the quality of the buffer/absorber interface.

Conclusions

Using an annealing process in which evaporated metallic precursors are successively submitted to a short selenization step and a long sulfurization step, it was possible to create CZGSSe absorber layers with sulfur inclusion going from 30 % to 100 % that have respective band gap of 1.45 eV to 2.0 eV. The results of these annealing procedures were reproducible and brought forth an almost pure kesterite with a controllable band gap. In addition to the linear dependence between sulfurization time and final sulfur inclusion, it was discovered that this sulfur inclusion is very slow. First, a primary mixed CZGSSe phase with a sulfur content of 30% has to form completely from the original pure CZGSe before higher sulfur inclusions can be achieved. This means it is impossible to produce single phase absorber layers with a

sulfur content lower than 30%. It was also discovered that the S/Se ratio is inhomogeneous through the thickness of the absorber, with top-layers, being more exposed to the H_2S atmosphere during annealing, showing sulfur inclusion up to 20% higher than the bulk material. In addition, SEM pictures of the absorber showed a deterioration of the aspect of the cell as more sulfur is included into the kesterite matrix. Indeed, crystals appear to become smaller, their outlines less sharp, and holes cover the whole surface and thickness of the absorber. Once more, these holes are potentially detrimental to the proper working of a potential finished product.

Tables

Sample	Cu/(Zn+Ge) (EDS)	Zn/Ge (EDS)	S/(S+Se) (EDS)	S/(S+Se) (XRD) (%)
17B3012$_2$	0.90	1.13	0.0	-1.0 ± 0.7
17B3108$_2$	0.91	1.23	0.58	54.7 ± 0.7
17B3101$_1$	0.83	1.00	0.95	97.9 ± 0.7

Tab. 1. Cation ratio results as well as S inclusion obtained using EDS measurements. The values of the S inclusion obtained by calculation from the XRD data is provided for these sample as a means of comparison.

Sample	Sulfurization Time (min)	Sulfur Inclusion (XRD) (%)
17B3169$_1$	50	53.3 ± 0.7
17B3173	50	48.4 ± 0.7
17B3174	50	51.9 ± 0.7
17B3175	50	52.6 ± 0.7
17B3176	50	51.2 ± 0.7
17B3177	50	58.2 ± 0.7
17B3178	50	57.5 ± 0.7

Tab. 2. Results of one of the reproducibility experiments showcasing 7 different samples that were annealed using the exact same recipe and their respective sulfur inclusions.

Figures
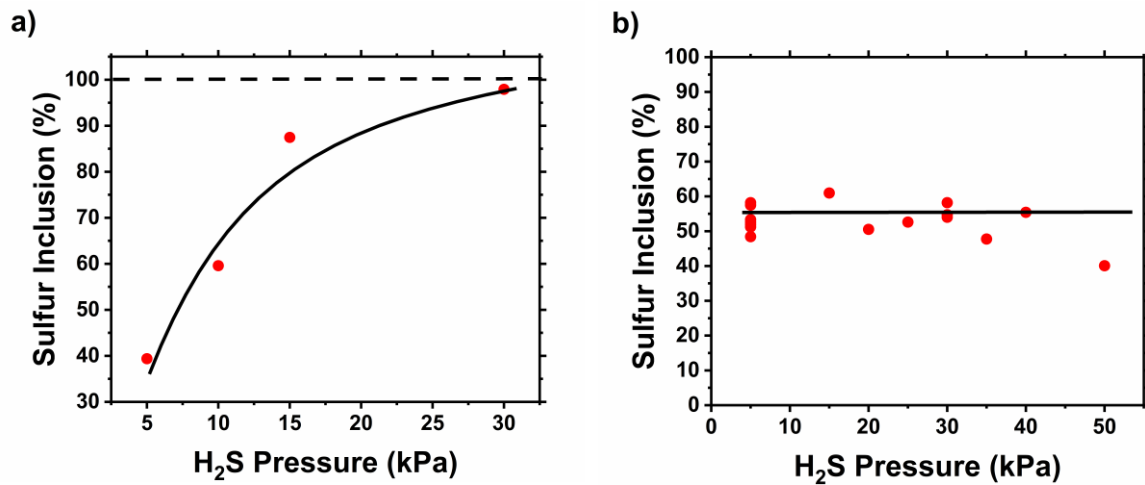
Fig. 1. Two graphs depicting the evolution of the sulfur inclusion as a function of the applied H_2S pressure during the sulfurization process. Inserted lines are guides to the eye and bear no direct physical meaning. a) Represents the case in which the regular refilling was not applied. All the samples presented in this graph were annealed for 120 min with the only varying parameter being the H_2S pressure. Graph b) shows the results obtained when using the recipes that include a regular refilling with gas of the reaction chamber. In this case, samples were annealed for 50 min at varying gas pressures.
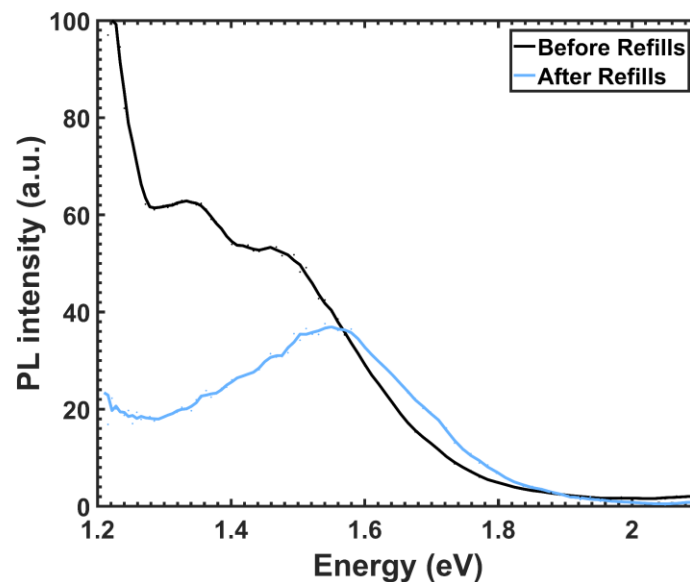
Fig. 2. PL spectra showcasing the effect of the addition of the refilling steps on the aspect of the photoluminescence spectrum. The signal from what is expected to be the main band gap is significantly increased and the general background noise is reduced. Both samples presented in the graph were sulfurized for 50 min in 30 kPa of H_2S but the second one (blue line on the graph) had a regular purge and refill cycle included in the recipe.
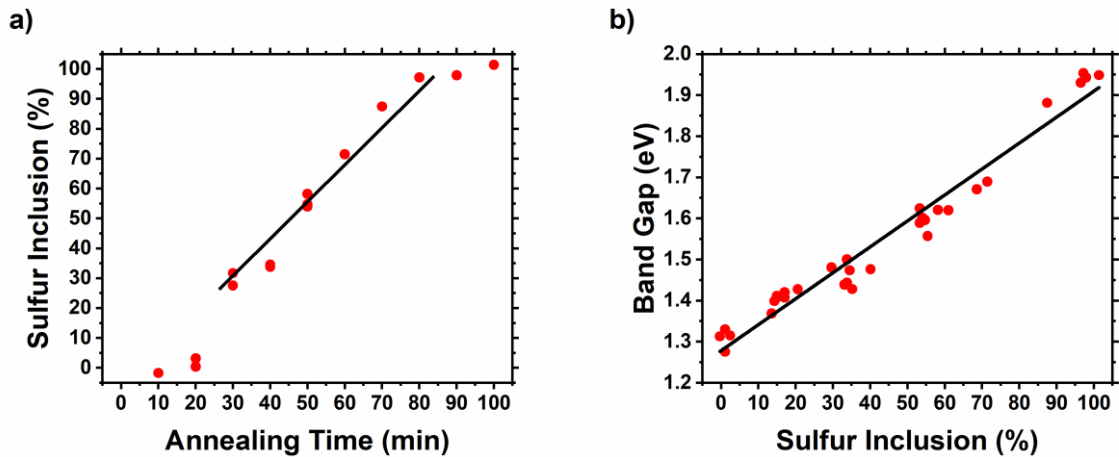
Fig. 3. a) Evolution of the sulfur inclusion with the annealing time in H_2S atmosphere. The samples were annealed at a temperature of 510°C and in a 30 kPa H_2S atmosphere, following the standard selenization. The data follows a fairly linear trend up to the saturation at 100% sulfur inclusion. Sulfur inclusion values were determined by XRD, using the shift in the (112) peak of the Kesterite phase, and double checked using EDS measurements. The black line is inserted solely as a guide to the eye and is not linked to a linear regression of the dataset. b) Evolution of the band gap value as a function of the sulfur inclusion. Inserted line represents the linear regression of the data set.
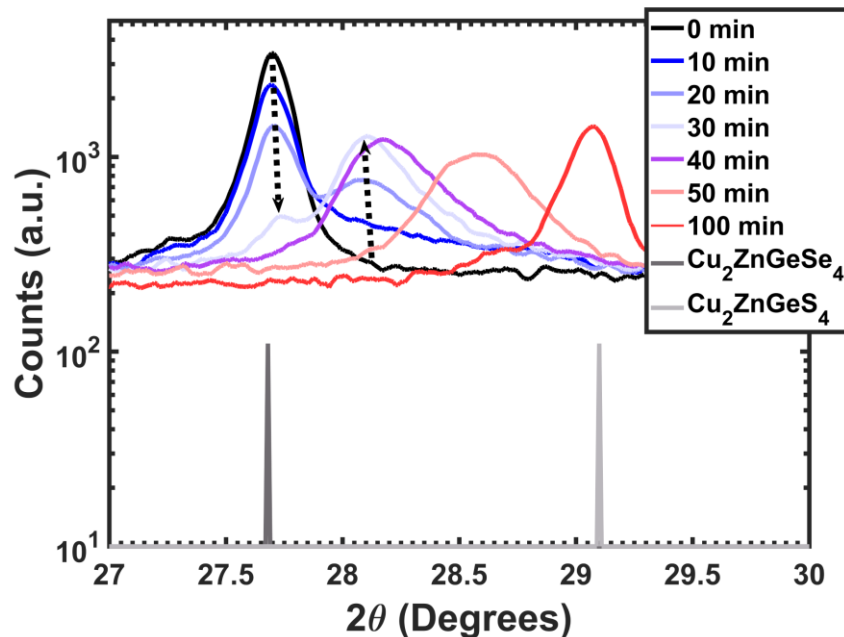
Fig. 4. XRD diffractograms exemplifying the progressive disappearance of the pure CZGSe phase in favor of an initial mixed CZGSSe phase at a sulfur content of about 30%. It can be seen that the transformation into the mixed phase is only complete after a sulfurization time of about 30-35 min. The narrow peaks at the bottom of the figures are reference diffractograms.
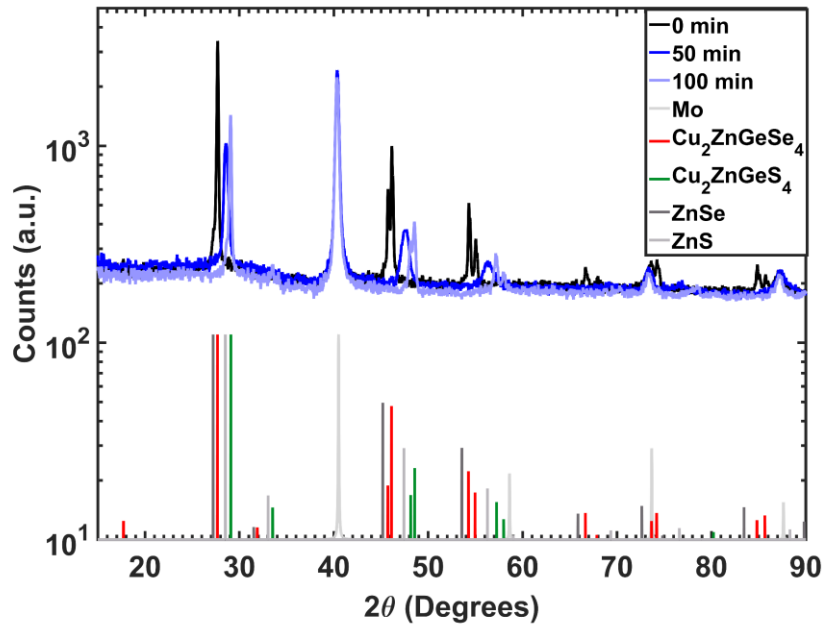
Fig. 5. Full XRD diffractograms of three different states of sulfurization. In black, the diffractogram of the original CZGSe phase, in dark blue, the diffractogram of a 50% mixed CZGSSe phase, and in light blue, the diffractogram of a CZGS phase. The diffractograms fit well to the expected CZGS references and seem to be almost pure kesterite. A small amount of ZnSe and ZnS seem to be present as well, mostly visible as a small shoulder on the (112) peak of the kesterite phases.
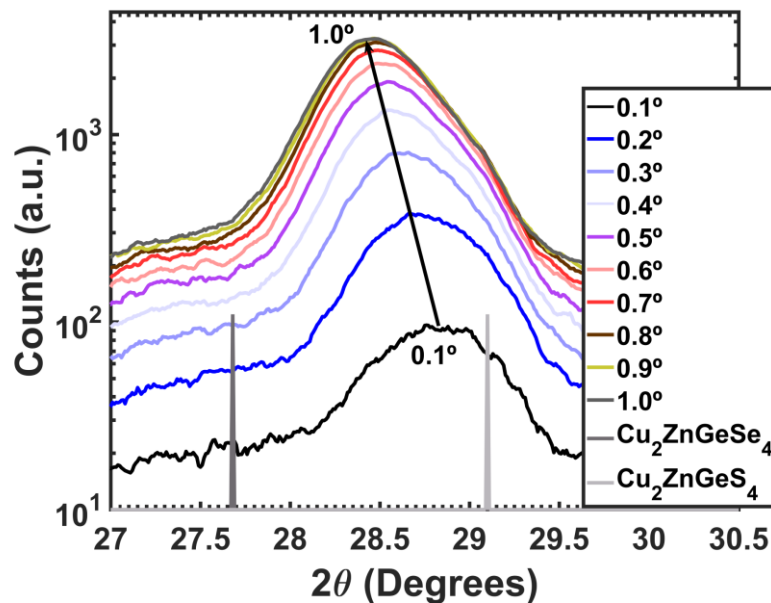

Fig. 6. XRD diffractograms exemplifying the evolution of the sulfur inclusion from the top layer down into the bulk material. The topmost layer is represented by the lowest diffractogram and when going up through the graphs, they represent ever deeper layers of the absorber layer. The narrow peaks at the bottom of the figures are reference diffractograms.
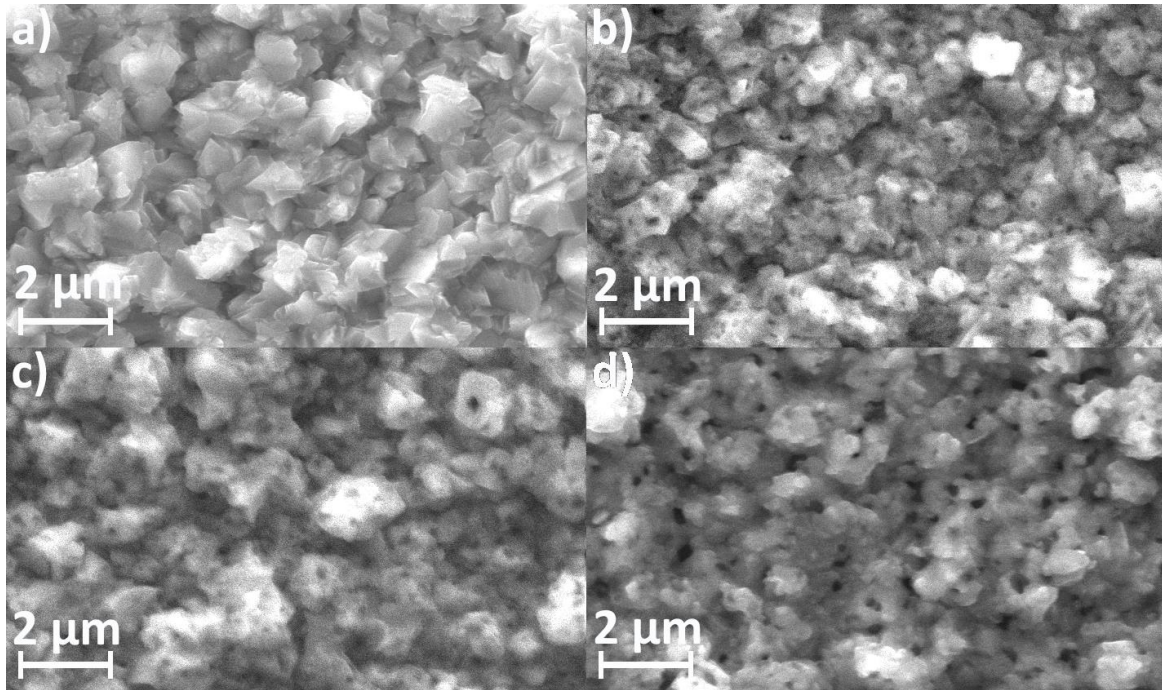
Fig. 7. Top - SEM images of the CZGS absorber layer at 4 different sulfur contents. a) Pure CZGSe with 0% sulfur content, b) CZGSSe with an approximated 35% of S, c) A CZGSSe sample containing approximately 60% of sulfur, and d) Pure CZGS with 100% of sulfur.
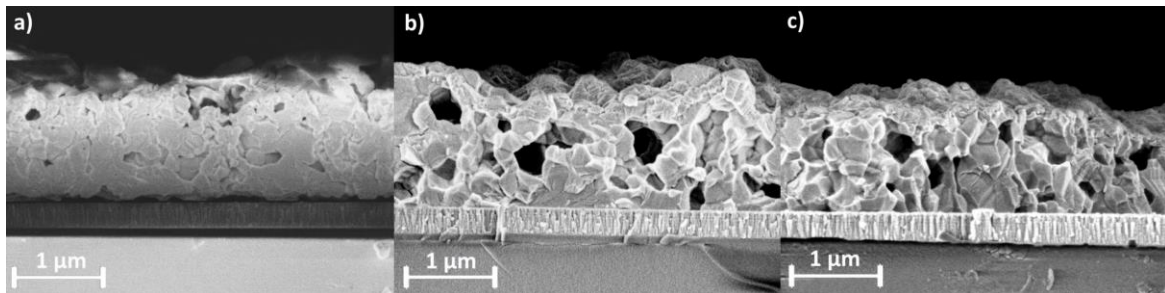

Fig. 8. Cross - SEM images of the CZGS absorber layer at 3 different sulfur contents. a) Pure CZGSe with a 0% sulfur content, b) CZGSSe with an approximated 50% of S, c) Pure CZGS with 100% of sulfur.

References

[1] International Energy Agency IEA, Solar Photovoltaic Energy, Technol. Roadmap. (2014) 60.

[2] T.P. Dhakal, C.–Y. Peng, R.R. Tobias, R. Dasharathy, C.R. Westgate, Characterization of a CZTS thin film solar cell grown by sputtering method, Sol. Ener. 100 (2014) 23-30. doi: 10.1016/j.solener.2013.11.035

[3] J. Tao, J. Liu, L. Chen, H. Cao, X. Meng, Y. Zhang, C. Zhang, L. Sun, P. Yang, J. Chu, 7.1% efficient co-electroplated Cu2ZnSnS4 thin film solar cells with sputtered CdS buffer layers, Gr. Chem. 18 (2016) 550-557. doi: 10.1039/C5GC02057C

[4] G. Brammertz, M. Buffière, S. Oueslati, H. ElAnzeery, K. Ben Messaoud, S. Sahayaraj, C. Köble, M. Meuris, J. Poortmans, Characterization of defects in 9.7% efficient Cu2ZnSnSe4-CdS-ZnO solar cells, Appl. Phys. Lett. 103 (2013) 163904. doi: 10.1063/1.4826448

[5] M. Buffière, G. Brammertz, M. Batuk, C. Verbist, D. Mangin, C. Koble, J. Hadermann, M. Meuris, J. Poortmans, Microstructural analysis of 9.7% efficient Cu2ZnSnSe4 thin film solar cells, Appl. Phys. Lett. 105 (2014) 183903. doi: 10.1063/1.4901401

[6] M.P. Suryawanshi, G.L. Agawane, S.M. Bhosale, S.W. Shin, P.S. Patil, J.H. Kim, A.V. Moholkar, CZTS based thin film solar cells: a status review, Mat. Tech. 28:1-2 (2013) 98-109. doi: 10.1179/1753555712Y.0000000038

[7] W. Shockley, H.J. Queisser, Detailed balance limit of efficiency of p-n junction solar cells, J. Appl. Phys. 32 (1961) 510–519. doi:10.1063/1.1736034.

[8] D.B. Khadka, J.H. Kim, Band gap engineering of alloyed Cu2ZnGexSn1-xQ4 (Q = S,Se) films for solar cell, J. Phys. Chem. C. 119 (2015) 1706–1713. doi:10.1021/jp510877g.

[9] S.C. Riha, B.A. Parkinson, A.L. Prieto, Compositionally Tunable Cu2ZnSn(S1–xSex)4 Nanocrystals: Probing the Effect of Se-Inclusion in Mixed Chalcogenide Thin Films, J. Am. Chem. Soc. 133 (2011) 15272-15275. doi: 10.1021/ja2058692

[10] M. Courel, T.G. Sanchez, N.R. Mathews, X. Mathew, Cu2ZnGeS4 thin films deposited by thermal evaporation: the impact of Ge concentration on physical properties, J Phys. D: App. Phys. 51 (2018). doi: 10.1088/1361-6463/aaa7db

[11] D.B. Kahdka, J. Kim, Study of structural and optical properties of Kesterite Cu2ZnGeX4 (X =S,Se) thin films synthesized by chemical spray pyrolysis, CrystEngComm.15 (2013) 10500–10509. doi:10.1039/C3CE41387J.

[12] S.P. Bremner, M.Y. Levy, C.B. Honsberg, Analysis of Tandem Solar Cell Efficiencies Under AM1.5G Spectrum Using a Rapid Flux Calculation Method, Prog. Photovolt. Res. Appl. 16 (2007) 225–233. doi:10.1002/pip.799.

[13] T. Schnabel, M. Seboui and E. Ahlswede, Evaluation of different metal salt solutions for the preparation of solar cells with wide-gap Cu2ZnGeSxSe4−x absorbers, RSC Adv. (2017), 7, 26-30. doi: 10.1039/C6RA23068G

[14] T. Schnabel, M. Seboui, A. Bauer, L. Choubrac, L. Arzel, S. Harel, N. Barreau, E. Ahlswede, Evaluation of different buffer materials for solar cells with wide-gap Cu2nGeSxSe4-x absorbers, RSC Adv. 7 (2017) 40105–40110. doi:10.1039/C7RA06438A.

[15] S. Sahayaraj, G. Brammertz, B. Vermang, T. Schnabel, E. Ahlswede, Z. Huang, S. Ranjbar, M. Meuris, J. Vleugels, J. Poortmans, Optoelectronic properties of thin film Cu2ZnGeSe4 solar cells, Sol. Energy Mater. Sol. Cells. 171 (2017) 136–141. doi:10.1016/j.solmat.2017.06.050.

[16] H. Matsushita, T. Ochiai, A. Katsui, Preparation and characterization of CuZnGeSe thin films by selenization method using the Cu–Zn–Ge evaporated layer precursors, J. Cryst. Growth (2005), 275, e995–e999, doi: 10.1016/j.jcrysgro.2004.11.154

[17] L. Huang, H. Deng, J. He, X. Meng, J. Tao, H. Cao, L. Sun, P. Yang, J. Chu, Cu content dependence of morphological, structural and optical properties for Cu2ZnGeS4 thin films synthesized by sulfurization of sputtered precursors, Mat. Lett 159 (2015) 1-4. doi: 10.1016/j.matlet.2015.05.170

[18] M. León, S. Levcenko, R. Serna, G. Gurieva, A. Nateprov, J. M. Merino, E. J. Friedrich, U. Fillat, S. Schorr, E. Arushanov, Optical constants of Cu2ZnGeS4 bulk crystals, J. Appl. Phys. 108 (2010) 093502. doi: 10.1063/1.3500439

[19] A. Tauc, J., Grigorovici, R., vancu, Tauc J Phy. stat. sol. 15, 627 (1966).pdf, Mater. Res. Bull. 3 (1966) 37–46. doi:10.1016/0025-5408(68)90023-8.

[20] J.J. Scragg, T. Ericson, T. Kubart, M. Edoff, C. Platzer-Björkman, Chemical Insights into the Instability of Cu2ZnSnS4Films during Annealing, Chem. Mater. 23 (2011) 4625–4633. doi:10.1021/cm202379s.

[21] J.J. Scragg, P.J. Dale, D. Colombara, L.M. Peter, Thermodynamic aspects of the synthesis of thin-film materials for solar cells, ChemPhysChem. 13 (2012) 3035–3046. doi:10.1002/cphc.201200067.

[22] E.V.C. Robert, J. de Wild, P.J. Dale, Reaction chemistry of group IV containing copper chalcogenide semiconductors Cu2MX3 (M = Sn, Ge and X = S, Se), J. Alloys Compd. 695 (2017) 1307–1316. doi:10.1016/j.jallcom.2016.10.271.

[23] R. Sun, M. Zhao, D. Zhuang, Q. Gong, L. Guo, L. Ouyang, Y. Wei, High-sulfur Cu2ZnSn(S,Se)4 films by sulfurizing as-deposited CZTSe film: The evolutions of phase, crystallinity and S/(S+Se) ratio, J. Alloys Compd. 695 (2017) 3139–3145. doi:10.1016/j.jallcom.2016.11.335.